Positively Charged Side Chains in Protein Farnesyltransferase Enhance Catalysis by Stabilizing the Formation of the Diphosphate Leaving Group†

Katherine E. Bowers and Carol A. Fierke*

Department of Chemistry, University of Michigan, Ann Arbor, Michigan 48109

Received January 23, 2004; Revised Manuscript Received March 3, 2004

ABSTRACT: Protein farnesyltransferase (FTase) requires both Zn^{2+} and Mg^{2+} for efficient catalysis of the formation of a thioether bond between carbon-1 of farnesyldiphosphate (FPP) and the cysteine thiolate contained in the carboxy-terminal CaaX sequence of target proteins. Millimolar concentrations of Mg^{2+} accelerate catalysis by as much as 700-fold in FTase. Although FTase lacks a typical DDXXD Mg^{2+} binding site found in other enzymes that use Mg^{2+} for diphosphate stabilization, D352β in FTase has been implicated in binding Mg^{2+} (Pickett et al. (2003) *J. Biol. Chem. 278*, 51243). Structural studies demonstrate that the diphosphate (PPi) group of FPP resides in a binding pocket made up of highly positively charged side chains, including residues R291β and K294β, prior to formation of an active conformation. Analysis of the Mg^{2+} dependence of FTase mutants demonstrates that these positively charged residues decrease the Mg^{2+} affinity up to 40-fold. In addition, these residues enhance the farnesylation rate constant by almost 80-fold in the presence of Mg^{2+}, indicating that these residues are not simply displaced by Mg^{2+} during the reaction. Mutations at R291β increase the pK_a observed in the magnesium affinity, suggesting that this arginine stabilizes the deprotonated form of the PPi leaving group. Furthermore, binding and catalysis data using farnesylmonophosphate (FMP) as a substrate indicate that the side chains of R291β and K294β interact mainly with the β-phosphate of FPP during the chemical reaction. These results allow refinement of the model of the Mg^{2+} binding site and demonstrate that positive charge stabilizes the developing charge on the diphosphate leaving group.

Protein farnesyltransferase (FTase)[1] catalyzes the attachment of a 15-carbon isoprenyl moiety onto a carboxyl-terminal cysteine residue contained within a signature "CaaX box" sequence of target proteins (*1*) (Figure 1). This posttranslational modification is critical for proper localization and stable membrane attachment of key signaling proteins, such as Ras, Rho, and nuclear lamins (*2*−*4*). Ras is a key component of a major cell-growth signaling pathway, and constitutively active mutants of Ras are found in 30% of all human cancers (*5*). The interaction of Ras with critical activators, such as GDP exchange factors and GTPase activating proteins, as well as its downstream targets within cell signaling pathways, is ultimately dictated by its localization to the plasma membrane (*2*−*6*). Without prenylation, Ras is maintained in the cytosol in an inactive state. A major effort over the past decade has been dedicated to discovering inhibitors of FTase that could attenuate Ras prenylation and activity and the aberrant signaling cascades that lead to tumorigenesis. Efforts to develop potent FTase inhibitors have been quite successful, producing several compounds showing promise in human clinical trials (*7*).

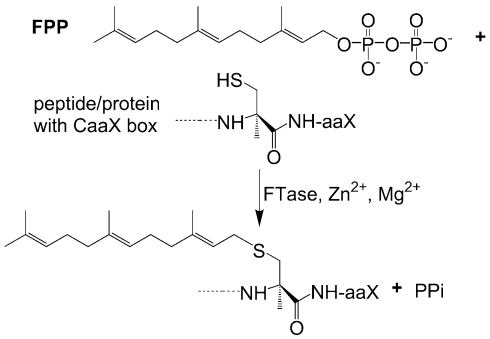

FIGURE 1: The overall reaction catalyzed by FTase. A thioether bond is formed between carbon-1 of FPP and the cysteine thiolate contained in the CaaX box sequence of target proteins.

The overall reaction catalyzed by FTase is depicted in Figure 1. The kinetics of this reaction have been extensively studied, demonstrating that the enzyme proceeds via a functionally ordered mechanism where farnesyldiphosphate (FPP) preferentially binds first to the enzyme, followed by

† This work was supported by a National Institutes of Health Postdoctoral Grant F32 CA84757 to K.E.B and a National Institutes of Health Grant GM40602 to C.A.F.

* To whom correspondence should be addressed. Mailing address: 930 N. University Ave, University of Michigan, Ann Arbor, MI 48109. Telephone: 734-936-2678. Fax: 734-647-4865. E-mail: fierke@umich.edu.

[1] Abbreviations: C-1, carbon-1 of FPP; CaaX, tetrapeptide sequence cysteine−aliphatic−aliphatic−X (serine, glutamine, methionine); CVFM, tetrapeptide sequence cysteine−valine−phenylalanine−methionine; DDXXD, Mg^{2+} binding motif with the sequence aspartate−aspartate−X−X−aspartate; Dns-GCVLS, dansylated pentapeptide sequence glycine−cysteine−valine−leucine−serine; EDTA, ethylenediaminetetraacetic acid; FMP, farnesylmonophosphate; FPP, farnesyldiphosphate; FTase, protein farnesyltransferase; FRET, fluorescence resonance energy transfer; GCVLS, pentapeptide sequence glycine−cysteine−valine−leucine−serine; I, FPT inhibitor II {(*E*,*E*)-2-[2-oxo-2-[[(3,7,11-trimethyl-2,6,10-dodecatrienyl)oxy]amino]ethyl]phosphonic acid, sodium}; PMSF, phenylmethylsulfonyl fluoride; PPi, diphosphate; TCEP, tris(2-carboxyethyl) phosphine hydrochloride; TKCVIM, hexapeptide sequence threonine−lysine−cysteine−valine−isoleucine−methionine; UPS, undecaprenyldiphosphate synthase; WT, wild-type.

10.1021/bi049822p CCC: $27.50
Published on Web 04/10/2004

binding of a CaaX sequence-containing peptide substrate (*8*, *9*). Upon the formation of the ternary complex, there is a high commitment to catalysis and products are formed rapidly and irreversibly with the concomitant release of a diphosphate product (PPi). The release of the farnesylated peptide product is the rate-limiting step in turnover with a k_{cat} value of 0.02 s^{-1} (*8*, *9*). During the reaction, the cysteine sulfur contained in the CaaX sequence reacts with carbon-1 (C-1) of FPP to form a thioether bond. The transition state for this reaction is hypothesized to have dissociative character with significant carbocation formation at C-1 of FPP (*8*, *10*). An active site zinc ion coordinates to the cysteine sulfur of the CaaX sequence, stabilizing a potent thiolate nucleophile at physiological pH (*11*, *12*). This zinc ion, as visualized in X-ray crystal structures of FTase, coordinates to residues D297β, C299β, and H362β (*13*, *14*). In addition to Zn^{2+}, millimolar levels of Mg^{2+} accelerate catalysis as much as 700-fold, indicating an important role for this divalent ion in stabilizing the chemical transition state. Similar to its role in other enzymes (*15*−*18*), the Mg^{2+} ion is proposed to stabilize the developing negative charge on the PPi leaving group, which in turn stabilizes carbocation formation at the C-1 position of FPP and facilitates nucleophilic attack by the thiolate (*8*, *19*). Consistent with this, transient kinetic studies have demonstrated that Mg^{2+} enhances a step at or before the chemical transition state with little effect on substrate binding or the product release rate constant (*8*).

Many crystal structures of binary and ternary complexes of FTase have been solved. Figure 2A illustrates the binding site of FPP within the active site of FTase, taken from the structure of a ternary complex of FTase with bound FPP and CVFM, a slow peptide substrate (*20*). Two distinct regions exist in the FPP binding site, a highly hydrophobic pocket in which the prenyl chain binds (not shown) and a region of highly positive charge in which the diphosphate moiety resides. This diphosphate binding pocket consists of residues K164α, H248β, R291β, K294β, and Y300β. In this structure, R291β makes a bidentate interaction with two of the nonbridging oxygens of PPi, and K294β interacts with a terminal oxygen atom on the β-phosphate. Mutations of these two residues (*21*) significantly affect the steady-state kinetic parameters causing an increase in K_m and alterations in k_{cat}, demonstrating their catalytic importance.

In other diphosphate utilizing enzymes, a catalytic magnesium ion is usually coordinated to negatively charged side chains, that is, a DDXXD motif, and the diphosphate group of the substrate (*17*). Several pieces of data suggest that Mg^{2+} coordinates the diphosphate of FPP bound to FTase. First, a crystal structure of Mn^{2+} bound to a complex of FTase with peptide (TKCVIM) and a FPP analogue that lacks a diphosphate moiety places one bound Mn^{2+} in the proximity of the diphosphate binding pocket (*14*). Second, kinetic studies demonstrate that the FTase-catalyzed reaction with farnesylmonophosphate (FMP) is not activated by Mg^{2+} and that the Mg^{2+} affinity for activation of the reaction with FPP decreases with protonation of the FPP substrate (*19*). On the other hand, no negatively charged side chains that could coordinate Mg^{2+} are observed in the immediate vicinity of the diphosphate binding pocket (*20*) (Figure 2). In fact, the positively charged residues of the diphosphate binding pocket are proposed to contribute to the decrease in affinity of the FPP diphosphate for Mg^{2+} when it binds to FTase (*22*).

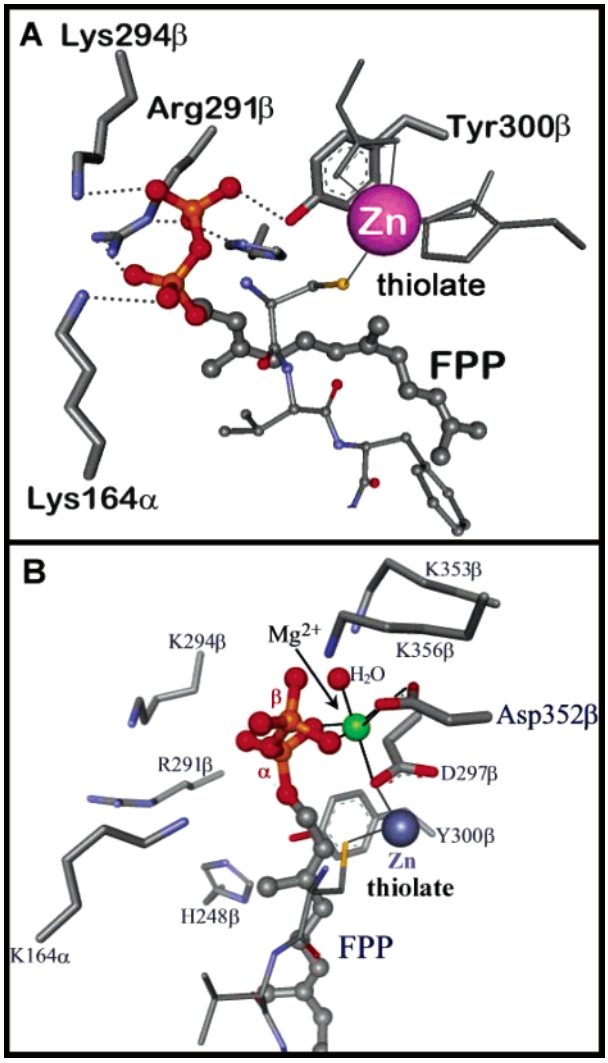

FIGURE 2: (A) X-ray crystal structure of the FPP binding site in FTase illustrating the diphosphate binding pocket consisting of residues K164α, H248β, R291β, K294β, and Y300β. A portion of the slow peptide substrate CVFM is also shown to illustrate its position relative to FPP, as well as the zinc coordination by the CaaX thiolate (*20*). (B) Model for the Mg^{2+} binding site of FTase formed in a reactive ternary complex (*14*, *22*, *23*).

However, recent crystallographic studies of the FTase−farnesylated peptide product complex suggest that the first two isoprene units of FPP adopt an altered conformation in an active substrate complex compared to their position in either the E−FPP or inactive E−FPP−peptide complex (*23*). This conformational change brings the C-1 of FPP close enough to the peptide thiolate to facilitate nucleophilic attack. Furthermore, mutagenesis studies of Y300β, K164α, and H248β demonstrate that the position of the diphosphate moiety is also shifted in this altered conformation (*24*). Finally, mutagenesis studies of D352β suggest that the bound Mg^{2+} ion coordinates the carboxylate side chain of this residue (*22*). Based on these data, a model for an active E−peptide−FPP−Mg^{2+} complex was proposed (Figure 2B, (*22*)). In this model, the diphosphate moiety moves out and away from the diphosphate binding pocket with little or no interaction with either R291β or K294β.

To further test this proposed model and to further investigate the catalytic function of the positive charge in the diphosphate binding site, we have investigated the

transient kinetic and thermodynamic binding properties of mutants at positions R291β and K294β FTase. These data clearly demonstrate that these residues have multiple functions, including decreasing the affinity of the catalytic Mg^{2+}, enhancing the affinity of FPP, and, most importantly, stabilizing the developing negative charge on the diphosphate leaving group in the catalytic transition state. Furthermore, these data are largely consistent with the proposed model for the active ternary complex conformation (Figure 2B (*24*)), although the side chains of R291β and K294β must interact with the β-phosphate of FPP to account for their role in stabilization of the leaving group during catalysis. R291β and K294β are located on a loop structure that is flanked by several glycine residues that could afford some conformational flexibility in this region. This would allow these side chains to maintain an interaction with the PPi moiety as the prenyl group rotates and the diphosphate moiety moves toward the Mg^{2+}-binding site.

The chemical transition state for FTase catalysis combines several features found in other enzymes that are involved in di- and triphosphate stabilization, including an aspartate-bridged dimetal center with Zn^{2+} and Mg^{2+}, similar to adenylate cyclase and enolase (*15*, *18*), and the presence of conserved lysine and arginine residues that act in concert with Mg^{2+} to stabilize a diphosphate leaving group, similar to undecaprenyldiphosphate synthase (*25*). As will be discussed, the emerging picture of the FTase chemical transition state involves a highly coordinated combination of metal coordination, substrate conformational movement, and charge stabilization to catalyze formation of the farnesylated peptide product.

MATERIALS AND METHODS

Miscellaneous. [1-^{3}H]-Farnesyldiphosphate (FPP) and [1-^{3}H]-farnesylmonophosphate were purchased from Amersham Biotech (Pistcataway, NJ) and American Radiolabeled Chemicals (St. Louis, MO), respectively, and used as supplied. The peptide GCVLS was synthesized and purified by Sigma-Genosys (St. Louis, MO), and the molecular weight was confirmed by electrospray mass spectrometry. FPT inhibitor II (I) {(*E*,*E*)-2-[2-oxo-2-[[(3,7,11-trimethyl-2,6,10-dodecatrienyl)oxy]amino]ethyl]phosphonic acid, sodium} was purchased from Calbiochem (San Diego, CA). All other chemicals were reagent grade. Assays were conducted at room temperature (21 °C).

Mutagenesis, Protein Expression, and Purification. Site-directed mutagenesis was carried out in the FPT/pET23a plasmid (*26*) using the Quik-Change kit from Stratagene (La Jolla, CA). The sequence of the mutated genes was determined by DNA sequencing (University of Michigan DNA Sequencing Core). Mutants at R291β include R291G, R291A, R291K, and R291Q FTase. Mutants of K294β include K294A and K294Q FTase. Protein expression was carried out in BL21(DE3) FPT/pET23a *Escherichia coli* as described previously (*26*). Cells from 2−4 L of growth media were resuspended in 50 mM Hepes−NaOH, pH 7.8, 10 μM $ZnCl_2$, 1 mM tris(2-carboxyethyl) phosphine hydrochloride (TCEP), and 10 μg/mL phenylmethylsulfonyl fluoride (PMSF). Cells were lysed by a single pass through a microfluidizer apparatus (Microfluidics, Newton, MA). The supernatant was clarified by centrifugation, then treated with a 0.1 volume of 10% (w/v) streptomycin sulfate at 4 °C. The supernatant was again clarified by centrifugation, followed by loading onto a Whatman DE52 anion-exchange column equilibrated in the above buffer (without PMSF) at room temperature. After the column was washed with buffer containing 100 mM NaCl, FTase was eluted with a linear gradient from 100 to 500 mM NaCl. Fractions containing FTase were pooled, concentrated, and dialyzed at 4 °C against the above buffer. FTase was further fractionated using a 20 mL POROS HQ column and the BioCad Sprint Chromatography Workstation (Applied Biosystems, Foster City, CA). The column was loaded and washed at room temperature in the same buffer as the DE52 column. FTase was eluted in a 200 mL 100−500 mM NaCl gradient. Fractions containing FTase, as judged by SDS−PAGE analysis, were pooled, concentrated, and diluted with buffer to lower the concentration of NaCl to <50 mM. Partially purified FTase was then loaded onto a 1.7 mL POROS HQ column and eluted with a 150 mL 100−450 mM NaCl gradient. Fractions containing the purest FTase (≥90%) were pooled, concentrated, and dialyzed at 4 °C against 50 mM Hepes−NaOH, pH 7.8, 2 mM TCEP. Enzyme stocks were stored at −80 °C.

To accurately determine the enzyme concentration, active site titrations were carried out. Increasing concentrations of dansyl-GCVLS peptide (Dns-GCVLS) were titrated into a solution containing ~500 nM enzyme and 10 μM FTase inhibitor II (Calbiochem) in 50 mM Heppso−NaOH, 5 mM $MgCl_2$, 2 mM TCEP, pH 7.8. After each addition of peptide, the sample was allowed to equilibrate at 25 °C for a total of 5 min. The binding of Dns-GCVLS to WT and mutant FTase enzyme was monitored by FRET (fluorescence resonance energy transfer) by exciting at 280 nm and measuring the emission from the dansyl group at 496 nm. Fluorescence measurements were made on a SLM-Aminco Bowman series 2 luminescence spectrometer using a 1 cm path length. Since the FTase concentration is much higher than the peptide K_D (*11*), the concentration of Dns-GCVLS needed to saturate the fluorescent signal at 496 nm indicates the concentration of FTase in the sample.

Peptide K_D. Dissociation constants for Dns-GCVLS were determined by monitoring FRET (*11*), as described above, at low FTase concentration. The assays contained 20 nM enzyme and 40 nM FTase inhibitor II, as a FPP analogue. Buffer conditions were 50 mM Heppso−NaOH, 1 mM $MgCl_2$, 2 mM TCEP, 10 nM EDTA, pH 7.8, with the ionic strength maintained at 0.1 M with the addition of NaCl. The change in the fluorescence signal as a function of Dns-GCVLS concentration was plotted, and eq 1 was fit to the

$$\Delta FL = \frac{EP}{1 + K_D/[\text{Dns-GCVLS}]_{total}} + IF \qquad (1)$$

data. In this equation, ΔFL is the observed fluorescence signal (after background correction) representing the concentration of E−I−peptide formed, EP is the fluorescence endpoint, IF is the initial fluorescence signal, K_D is the calculated dissociation constant, and $[\text{Dns-GCVLS}]_{total}$ is the peptide concentration.

FMP and FPP K_D by Equilibrium Dialysis. Farnesylmonophosphate (FMP) and FPP dissociation constants were measured by equilibrium dialysis in the following manner. One side of the dialysis unit (E side) contained 1 mL of

enzyme plus a fixed concentration of [1-^{3}H]-FPP (10 nM for WT and 20 nM for mutants) or [1-^{3}H]-FMP (30 nM) and the other side (FP_n side) contained 1 mL of [1-^{3}H]-FPP or [1-^{3}H]-FMP at the same concentration. The buffer for all equilibrium dialysis experiments was 50 mM Heppso−NaOH, 5 mM $MgCl_2$, 2 mM TCEP, pH 7.8. The two sides were separated by a 25 kDa molecular weight dialysis membrane (Spectra/Por 7, Spectrum Laboratories, Rancho Dominguez, CA), allowing equilibration of FPP between the compartments but isolating the enzyme in one side. In this assay, the enzyme concentration was varied (2−3000 nM), and the fraction of E−FPP or E−FMP formed as a function of total enzyme concentration was calculated from the radioactivity in the two chambers using eq 2 (where FP_n signifies either FPP or FMP). The value of $[E-FP_n]/[FP_n]_{total}$

$$[E-FP_n]/[FP_n]_{total} = (CPM_{E\ side} - CPM_{FP_n\ side})/(CPM_{E\ side} + CPM_{FP_n\ side}) \quad (2)$$

(fraction of FP_n bound) was then plotted as a function of $[E]_{free}$, and eq 3 was fit to the data. In eq 3, EP is equal to

$$\frac{[E-FP_n]}{[FP_n]_{total}} = \frac{EP}{1 + (K_D)^n/([E]_{free})^n} \quad (3)$$

the fraction of FP_n bound at saturation, K_D is the FP_n dissociation constant, and n indicates binding cooperativity. For all of the fits presented in this manuscript, we used $n = 1$. However, for FPP measurements, the value of n varied from experiment to experiment from 1 to 1.4, likely due to the uncertainties of determining the concentrations of $[FPP]_{free}$ and $[E]_{free}$.

Single Turnover Kinetics. To measure the effect of mutations on the chemical reaction rate constant (k_{chem}), single turnover reactions were performed. The buffer for these experiments was 50 mM Heppso−NaOH, 2 mM TCEP, pH 7.8, with the ionic strength maintained at 0.2 M with NaCl. For measuring the k_{chem} value in the presence of saturating [Mg^{2+}], a 5−50 mM concentration of $MgCl_2$ (depending upon the mutant) was added and the ionic strength maintained accordingly. For reactions performed on the benchtop ($k_{chem} < 0.1\ s^{-1}$), a 10 μL volume containing 600 nM enzyme and 150 nM [1-^{3}H]-FPP was rapidly mixed with 5 μL of 300 μM GCVLS to give final concentrations of 400 nM E, 100 nM [1-^{3}H]-FPP, and 100 μM GCVLS. After the desired reaction time, 15 μL of 100% 2-propanol was added to quench the reaction, and the sample was placed on ice. For reactions having $k_{chem} > 0.1\ s^{-1}$, a quench-flow apparatus (Kintek Corp, Austin, TX) was used. In these reactions, 15 μL containing 800 nM E and 200 nM [1-^{3}H]-FPP was rapidly mixed with 15 μL of 200 μM GCVLS to give final concentrations identical to those used in the benchtop experiments. After the desired reaction time, reactions were quenched by addition of 90 μL of 20% acetic acid/80% 2-propanol. Samples were either loaded directly onto thin-layer chromatography (TLC) plates or dried and resuspended in 50% 2-propanol/H_2O prior to loading. Product and unreacted [1-^{3}H]-FPP were separated on Whatman PE SIL G TLC plates in an 8:1:1 2-propanol/NH_4OH/H_2O mobile phase. Corresponding bands were cut from the TLC plate, and the radioactivity of each band was quantified by scintillation counting. The fraction product formed at each time point was calculated by dividing the product CPM (counts per minute) value by the total CPM value. The fraction product was then plotted as function of reaction time, t, and eq 4 was fit to the data to calculate the first-order rate

$$\text{fraction product} = EP(1 - e^{-k_{chem}t}) + C_0 \quad (4)$$

constant of chemistry, k_{chem}. In eq 4, EP is equal to the fraction product end point, and C_0 is the fraction product at $t = 0$.

Measurement of K_{Mg}. The dependence of k_{chem} on Mg^{2+} concentration for all mutants was measured at pH 7.8 to determine the apparent dissociation constant for Mg^{2+}, K_{Mg}. Single turnover assays, as described above, were performed in the presence of 0−50 mM $MgCl_2$ in 50 mM Heppso−NaOH, 2 mM TCEP, pH 7.8, with the ionic strength maintained at 0.2 M with NaCl. Equation 4 was fit to each individual time course at a given Mg^{2+} concentration, and eq 5 was then fit to the aggregate data, where k_{obs} is k_{chem}

$$k_{obs} = \frac{k_{max}}{1 + K_{Mg}/[Mg^{2+}]} + k_0 \quad (5)$$

(eq 4), k_0 is the rate constant in the absence of magnesium, and k_{max} is the rate constant at saturating magnesium concentration.

The effect of pH on the K_{Mg} value was also determined by single turnover kinetics. All assays contained 400 nM E, 100 nM [1-^{3}H]-FPP, and 100 μM GCLVS in 50 mM buffer, 2 mM TCEP with the ionic strength maintained at 0.2 M with NaCl. Buffers used were MES−NaOH (pH 5.8−6.0), BES−NaOH (pH 6.0−6.6), Heppso−NaOH (pH 6.6−8.5), and Bicine−NaOH (pH 8.5−9.1). The value of K_{Mg} at pH values ranging from 5.8 to 9.1 was obtained as described above. Equation 6 was fit to the K_{Mg} as a function of pH

$$K_{Mg} = K_{1/2}(1 + 10^{pK_a - pH}) \quad (6)$$

data, where $K_{1/2}$ equals the pH-independent apparent dissociation constant.

FMP Single Turnover Reaction. The farnesylation rate constant using FMP as a substrate was measured by single turnover kinetics. Assays were performed on the benchtop by rapidly mixing 10 μL of E−[1-^{3}H]-FMP and 5 μL of GCVLS to final concentrations of 400 nM E, 100 nM [1-^{3}H]-FMP, and 100 μM GCVLS. The buffer for these experiments was 50 mM MES−NaOH, 5 mM $MgCl_2$, 2 mM TCEP, pH 5.8 (pH maximum for the WT reaction with FMP (*19*)). Reactions were quenched with the addition of 15 μL of 100% 2-propanol and set on ice. Samples were processed as described above for single turnover kinetics. Equation 4 was fit to these data to obtain k_{chem} values.

Multiple Turnover Kinetics. The steady-state kinetic parameter, k_{cat}, was measured at saturating peptide and FPP concentrations. Assays were performed on the benchtop by rapidly mixing 10 μL of GCVLS and [1-^{3}H]-FPP with 5 μL of enzyme to final concentrations of 24 nM FTase, 1 μM [1-^{3}H]-FPP, and 10 μM GCVLS in 50 mM Heppso−NaOH, 5 mM $MgCl_2$, 2 mM TCEP, pH 7.8. Reactions were quenched with the addition of 15 μL of 20% (v/v) acetic acid/80% 2-propanol and set on ice. Samples were processed

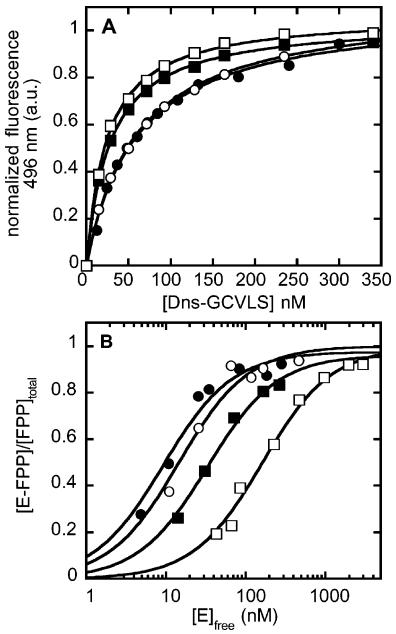

FIGURE 3: Substrate binding to WT and mutant FTase. Panel A shows Dns-GCVLS binding titrations for WT (●), R291G (○), R291K (■), and K294A(□) FTase measured by FRET emission at 496 nm after excitation at 280 nm. Assays contained 20 nM enzyme and 40 nM FTase inhibitor II in 50 mM Heppso−NaOH, 1 mM $MgCl_2$, 2 mM TCEP, 10 nM EDTA, pH 7.8, with the ionic strength maintained at 0.1 M with NaCl. A binding isotherm (eq 1) has been fit to the data, and resulting K_D values are given in Table 1. Panel B shows FPP binding data from equilibrium dialysis for WT (●), R291Q (□), R291A (■), and K294Q (○) FTase. The FPP dissociation constants were determined as described in Materials and Methods with 2−3000 nM enzyme and either 10 (WT) or 20 nM (mutants) [1-^{3}H]-FPP on both sides of the dialysis unit. Buffer conditions were 50 mM Heppso−NaOH, 5 mM $MgCl_2$, 2 mM TCEP, pH 7.8. For clarity, the experimentally determined endpoints (0.92−1.03) were normalized to 1. FPP K_D values were determined using eq 3 and are listed in Table 1.

as described above for single turnover kinetics. The initial rate was calculated from a linear fit of product formation taken from the first 10% of the reaction. The initial rate divided by the total enzyme concentration yielded k_{cat}.

RESULTS

Selection of Mutations. The focus of this study was to discern the role of the positively charged diphosphate binding pocket during reactions catalyzed by FTase. This region of the active site is responsible for interacting with the PPi moiety of FPP (Figure 2A). Specifically, mutations at positions R291β and K294β were examined for their effects on FPP binding, Mg^{2+} affinity, and chemical rate constant. All mutations, except R291K, were chosen to remove the positive charge functionality of these residues, with the glutamine replacements chosen to maintain a similar van der Waals radius of the mutated side chain. The lysine replacement at R291β was chosen to test the activity of a side chain capable of making only a single positive-charge interaction with the PPi moiety of FPP.

Effect of Mutations on Substrate Binding. Dissociation constants for the peptide substrate, Dns-GCVLS, were measured by FRET by titrating increasing amounts of the peptide into a known concentration of enzyme−inhibitor complex. Figure 3A illustrates the binding curves for representative enzymes R291G, R291K, K294A, and WT FTase, presented as normalized fluorescence for clarity. As listed in Table 1, the peptide K_D for WT FTase is 59 ± 3 nM. The R291G, R291Q, and K294Q mutations alter this value little with K_D values of 62 ± 3, 65 ± 9, and 48 ± 2 nM, respectively. For R291K and K294A FTase, the peptide has a slightly higher affinity with K_D values of 28 ± 1 and 24 ± 1 nM, respectively. Conversely, the R291A mutation lowers the peptide affinity about 2-fold with a K_D value of 104 ± 15 nM. These results indicate that the side chains of R291β and K294β contribute little to peptide affinity in the E−I−peptide complex.

The FPP dissociation constants for WT and mutant enzymes were measured by equilibrium dialysis as described in Materials and Methods. Figure 3B illustrates plots of $[E-FPP]/[FPP]_{total}$ (fraction of FPP bound) as a function of $[E]_{free}$ for WT, R291A, R291Q, and K294Q FTase. As listed in Table 1, WT has a K_D for FPP binding of 10 ± 2 nM. Deletion of the R291 side chain (R291A and R291G FTase) decreases the FPP affinity 3−4-fold with K_D values of 41 ± 9 and 31 ± 5 nM, respectively. FPP affinity also decreases for replacement of the arginine side chain with lysine (7-fold, K_D = 68 ± 7 nM) and glutamine (17-fold, 170 ± 20 nM). The K294Q and K294A mutations lower the FPP affinity 2-fold (15 ± 3 nM) and 7-fold (51 ± 10 nM), respectively. These results indicate that the side chains of R291β and K294β play a role in stabilizing the E−FPP complex. Complete removal of either of the positively charged side chains decreases the affinity at most 7-fold. The enhancement of FPP affinity afforded by these side chains is comparable to the value expected for formation of a solvent-exposed salt bridge (*27*) consistent with the partially solvent-exposed surface of the PPi binding pocket. At position 291, the structure of the side chain, not just the positive charge, is important for FPP affinity since the affinity of the R291K and R291Q mutants is weaker than that of R291A. The glutamine replacement at R291β may adopt a conformation that sterically hinders effective binding of the PPi moiety, leading to disruption of the interaction of a portion of the prenyl chain with the active site. In summary, these data suggest that charge interactions with the diphosphate group modestly enhance binding; however, hydrophobic interactions with the isoprenyl chain must also be important for achieving the nanomolar affinity of FPP.

Effect of Mutations on k_{chem} in the Absence of Mg^{2+}. The rate constant for farnesylation was measured for WT and mutants by single turnover kinetics at pH 7.8 in the absence of Mg^{2+}. The fraction product formed as a function of time was measured (not shown), and a first-order exponential (eq 4) was fit to the data. The resulting k_{chem} values are listed in Table 1. WT FTase in the absence of Mg^{2+} has a k_{chem} value of 0.008 ± 0.0004 s^{-1} (Figure 4, inset). Complete removal of the side chain at position 291 (A or G) or 294 (A) decreases the farnesylation rate constant by 20-fold or 4-fold, respectively, demonstrating that these side chains stabilize the transition state. However, at position 291, much of the effect of side chain deletion can be ameliorated by the R291Q or R291K substitutions where the farnesylation rate constant is only decreased 3−8-fold, respectively. This suggests that in the absence of Mg^{2+}, this side chain may play an important role in positioning the two substrates, as well as stabilizing the developing negative charge in the transition state. The deleterious effects of these mutations on farnesylation are

Table 1: Binding Affinity and Kinetic Values for WT and Mutant FTase[a]

mutant	K_D^{FPP} (nM)	$K_D^{Dns-GCVLS}$ (nM)	$k_{chem} \times 10^3$ s^{-1} minus Mg^{2+}	k_{max} (s^{-1})[b]	k_{cat} (s^{-1})	K_{Mg}, pH 7.8 (mM)
WT	10 ± 2	59 ± 3	8.0 ± 0.4	4.7 ± 0.2	0.022 ± 0.001[c]	4.9 ± 0.8[d]
R291A	41 ± 9	104 ± 15	0.4 ± 0.03	0.09 ± 0.003	0.013 ± 0.001	1.0 ± 0.05
R291G	31 ± 5	62 ± 3	0.4 ± 0.02	0.06 ± 0.001	0.015 ± 0.002	1.1 ± 0.04
R291K	68 ± 7	28 ± 1	1.0 ± 0.05	0.35 ± 0.004	0.057 ± 0.008	24 ± 0.6
R291Q	170 ± 20	65 ± 9	2.5 ± 0.2	0.06 ± 0.002	0.064 ± 0.005	0.1 ± 0.01
K294A	51 ± 10	24 ± 1	1.9 ± 0.1	0.24 ± 0.01	0.025 ± 0.002	0.3 ± 0.02
K294Q	15 ± 3	48 ± 2	0.5 ± 0.02	0.10 ± 0.003	0.024 ± 0.001	0.6 ± 0.03

[a] Conditions: 50 mM Heppso, 2 mM TCEP, pH 7.8; ionic strength 0.2 M with NaCl; room temperature. [b] k_{max} is the farnesylation rate constant in the presence of saturating Mg^{2+} concentration at pH 7.8. [c] Data taken from ref *8*. [d] Data taken from ref *19*.

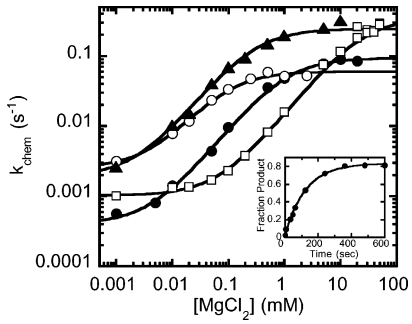

FIGURE 4: The dependence of k_{chem} on $MgCl_2$ concentration at pH 7.8. Individual time courses of fraction product formed as a function of time under single turnover conditions were measured for R291A (●), R291K (□), R291Q (○), and K294A (▲) FTase at pH 7.8. Assay conditions were 400 nM enzyme, 100 nM [1-^{3}H]-FPP, and 100 μM GCLVS in 50 mM Heppso−NaOH, 0−50 mM $MgCl_2$, 2 mM TCEP, pH 7.8 with the ionic strength maintained at 0.2 M with NaCl. The values of k_{chem} were determined from fitting a single-exponential decay (eq 4) to the data. The values of k_{max} and K_{Mg} (Table 1) were determined from a fit of eq 5 to the Mg^{2+}-dependence of k_{chem}. The inset shows a single turnover reaction for WT FTase at 0 mM $MgCl_2$. The value of k_{chem} was determined by fitting eq 4 to these data.

larger in the presence of Mg^{2+} (see below). Therefore, it is plausible that the transition state for farnesylation in the absence of Mg^{2+} is altered; perhaps the carbocation character and developing negative charge on the diphosphate leaving group decreases or a conformational change becomes partially rate-limiting.

Effect of Mutations on K_{Mg} and k_{chem} at Saturating Mg^{2+}. The effect of mutations in the diphosphate binding pocket on the farnesylation rate constant at saturating Mg^{2+} concentration and on the apparent Mg^{2+} affinity at pH 7.8 were measured by carrying out single turnover kinetics as a function of Mg^{2+} concentration. Figure 4 is a plot of the k_{chem} values for representative enzymes (R291A, R291K, R291Q, and K294A FTase) as a function of Mg^{2+} concentration. The values of k_{max}, the farnesylation rate constant at saturating Mg^{2+} concentration, and K_{Mg} were calculated from a fit of eq 5 to these data (Figure 4, Table 1). Mutations at positions 291 and 294 clearly affect both k_{max} and K_{Mg}. Deletion of the side chains at positions 291 (A, G) and 294 (A) decrease farnesylation 52−78-fold and 20-fold, respectively, demonstrating that these side chains significantly enhance catalysis in the presence of saturating Mg^{2+}. At both positions, the mutants with glutamine substitutions (R291Q and K294Q) have farnesylation rate constants that are equal to or lower than the alanine substitutions, suggesting that interaction with the positive charge of the side chain is the major factor enhancing catalysis. However, the farnesylation

Scheme 1 : The Relationship between Deprotonation of the Diphosphate Group of FPP and Mg^{2+} Affinity in the E−FPP Complex

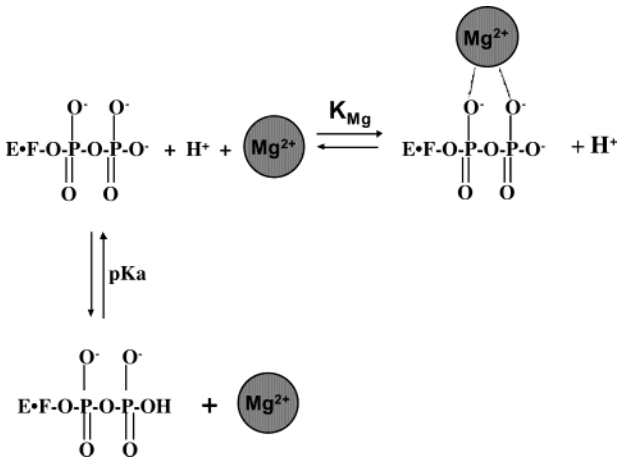

rate constant of the R291K mutant is still 13-fold slower than WT, indicating that the arginine side chain may also make important hydrogen bonding interactions that stabilize the transition state. These data provide clear evidence that interaction of the diphosphate of FPP with Mg^{2+} does not simply replace the interaction with the positively charged side chains in the binding pocket. The dominant role of these side chains in catalysis could be stabilizing an active conformation of the FPP substrate in the active site, stabilizing developing charge on the diphosphate leaving group, or a combination of both.

In addition, all mutations that decrease the positive charge in the diphosphate binding pocket also decrease the value of K_{Mg}, compared to WT (4.9 mM (*19*)). Deletion of the side chain in R291A (1.0 ± 0.05 mM), R291G (1.1 ± 0.04 mM), and K294A (0.3 ± 0.02 mM) enhances the apparent Mg^{2+} affinity 5-, 5-, and 16-fold, respectively. The R291Q mutation has the most dramatic effect with a K_{Mg} of 0.1 ± 0.01 mM, resulting in a 50-fold enhancement in the apparent Mg^{2+} affinity. In contrast, in a mutant where the positive charge is maintained (R291K), the apparent K_{Mg} value is 24 ± 0.6 mM, approximately 5-fold higher than WT FTase. Collectively, these results indicate that the positively charged residues of the PPi binding pocket diminish the apparent Mg^{2+} affinity in the WT enzyme. Removal of the positive charge functionality of R291β and K294β allows Mg^{2+} to more effectively compete for coordination to the PPi moiety, due to weakening of the interactions with the positively charged side chains in the binding pocket and decreasing charge repulsion on Mg^{2+} from the positively charged pocket.

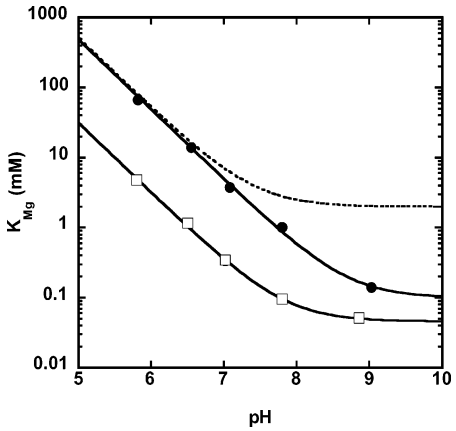

FIGURE 5: The effect of pH on K_{Mg}. K_{Mg} constants were measured at pH values ranging from 5.8 to 9.0 for R291A (●) and R291Q (□) FTase as described in Materials and Methods and the caption of Figure 4. Equation 6 has been fit to the data, and resulting pK_a and $K_{1/2}$ values are listed in Table 2. WT data (dotted line) is taken from ref *19*.

Table 2: Values for $K_{1/2}$ Mg^{2+} and pK_a[a]

mutant	$K_{1/2}$ Mg^{2+} (mM)	pK_a
WT	2.0 ± 0.2[b]	7.4 ± 0.1[b]
R291A	0.1 ± 0.01	8.7 ± 0.05
R291Q	0.05 ± 0.006	7.8 ± 0.1

[a] Measured in 50 mM buffer, 2 mM TCEP, ionic strength of 0.2 M with NaCl, room temperature. [b] Data taken from ref *19*.

Despite the apparent increase in Mg^{2+} affinity of the mutants (except R291K), the farnesylation rate constant decreases.

Effect of R291Q and R291A on the Mg^{2+}-Dependent pK_a of WT FTase. To examine more closely the cause of the lowered catalytic activity of the mutants, we examined the pH dependence of K_{Mg} with R291A and R291Q FTase. These experiments were carried out to test the effect of the arginine side chain on the pK_a proposed to represent the deprotonation of a PPi oxygen (Scheme 1 (*19*)). To this end, a series of K_{Mg} titrations (as described in Figure 5) as a function of pH were carried out for the R291Q and R291A mutants (data not shown). The pH dependence of K_{Mg} is shown in Figure 5; eq 6 was fit to the data and resulting values for $K_{1/2}$, the pH-independent apparent Mg^{2+} affinity, and pK_a are listed in Table 2. For WT, the values are $K_{1/2}$ of 2.0 ± 0.2 mM and a Mg^{2+}-dependent pK_a of 7.4 ± 0.1 (*19*). The value of $K_{1/2}$ decreases even more than the K_{Mg} value at pH 7.8 (above) for mutations at position 291; $K_{1/2}$ decreases dramatically by 40- and 20-fold for R291Q (0.05 ± 0.006 mM) and R291A (0.1 ± 0.01 mM) FTase, respectively. Additionally, the values for the Mg^{2+}-dependent pK_a are shifted to higher pH by 0.4 pH units for R291Q (7.8 ± 0.1) and 1.3 units for R291A FTase (8.7 ± 0.05). In both the WT and mutant enzymes, this ionization, presumed to reflect deprotonation of the PPi moiety, is coupled to enhanced Mg^{2+} affinity (Scheme 1). These data demonstrate that the side chain of R291β not only is a significant modulator of Mg^{2+} affinity but also plays a key role in stabilizing the charge of the deprotonated form of bound FPP. This effect would also translate into stabilization of the developing negative charge on the PPi moiety during the transition state of this reaction. The loss of the arginine side chain in the R291A and R291Q mutants causes a stabilization of the protonated form of the PPi moiety of bound FPP relative to the deprotonated form,

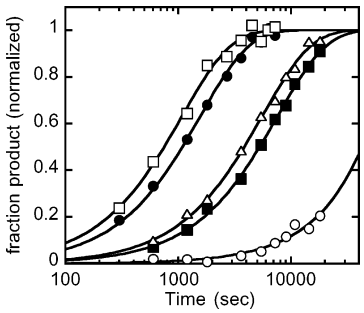

FIGURE 6: FMP turnover. Single turnover reactions with FMP catalyzed by WT (●), R291A (○), R291G (■), R291Q (□), and K294A (△) FTase are measured. Assays contained 400 nM enzyme, 100 nM [1-^{3}H]-FMP, and 100 μM GCVLS in 50 mM MES−NaOH, 5 mM $MgCl_2$, 2 mM TCEP, pH 5.8. Data are presented as normalized fraction product formed as a function of time, and eq 4 has been fit to the data. R291A FTase data has been analyzed with a linear equation to estimate k_{chem} from the initial velocity. Resulting k_{chem} values are listed in Table 3.

Table 3: FMP Data

mutant	$k_{chem} \times 10^4$ (s^{-1})[a]	K_D (nM)[b]
WT	6.4 ± 0.3	92 ± 15
R291A	~0.14[c]	34 ± 3
R291G	1.3 ± 0.07	*d*
R291K	2.5 ± 0.1	*d*
R291Q	9.5 ± 0.5	58 ± 9
K294A	2.0 ± 0.1	*d*
K294Q	2.4 ± 0.1	*d*

[a] Conditions: 50 mM Mes−NaOH, 5 mM $MgCl_2$, 2 mM TCEP, pH 5.8. [b] Conditions: 50 mM Heppso−NaOH, 5 mM $MgCl_2$, 2 mM TCEP, pH 7.8. [c] Value was calculated from initial rate. [d] Not determined.

as evident in the shift of the pK_a values to higher pH. However, comparison of the results for the alanine and glutamine substitutions indicates that the positive charge of the R291 side chain is not the only stabilizing factor, because the glutamine replacement affects the Mg^{2+}-dependent pK_a to a lesser extent. The FPP substrate undergoes significant conformational movement in the formation of the reactive state (Figure 2B), and it is plausible that the R291 side chain also stabilizes this conformational change by a combination of side chain packing and lowered solvent accessibility, characteristics that would be better maintained in the R291Q mutant.

Effect of Mutations on FMP Catalysis and Binding. The reactivity of FMP as a substrate for FTase compared to FPP can be used to probe the interaction of mutated residues with the α- and β-phosphates of FPP, as has been shown with other mutants (*22*, *24*). Figure 6 illustrates the single turnover kinetics of FMP catalyzed by representative enzymes WT, R291A, R291G, R291Q, and K294A FTase. Values for k_{chem} are listed in Table 3. WT catalyzes farnesylation, using FMP as the substrate, slowly with a rate constant of $(6.4 \pm 0.3) \times 10^{-4}$ s^{-1}. The crystal structure indicates that R291β makes a bidentate interaction with two of the nonbridging oxygens of PPi, while K294β interacts with a terminal oxygen atom on the β-phosphate (*20*). Assuming that FMP binds similarly to FPP, mutations at K294 should have little effect on reactivity, while mutations at R291 should have a smaller effect on the FMP reactivity compared to that of FPP. As predicted, the majority of the mutations (all except R291A) either modestly increase (1.5-fold, R291Q) or decrease (<5-fold) the value of k_{chem} with FMP. In fact, these mutations

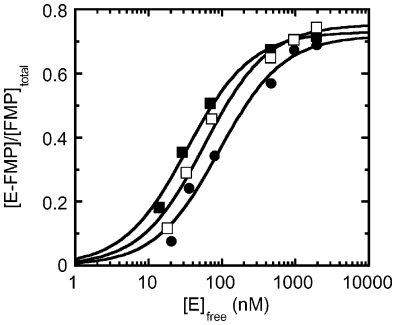

FIGURE 7: FMP binding data obtained by equilibrium dialysis. The FMP dissociation constants for WT (●), R921A (■), and R291Q (□) FTase were determined as described in Materials and Methods with 25−2000 nM enzyme and 30 nM [1-^{3}H]-FMP (on both sides of the dialysis unit). Buffer conditions were 50 mM Heppso−NaOH, 5 mM $MgCl_2$, 2 mM TCEP, pH 7.8. FMP K_D values were determined using eq 3 and are listed in Table 3.

in FTase affect the reactivity of FMP significantly less than that of FPP−Mg^{2+}. R291A FTase is the only mutation, including R291G, which significantly decreases reactivity with FMP for reasons that are currently unclear. The k_{chem} value for this mutant was calculated from the initial rate to be $\sim 1.4 \times 10^{-5}$ s^{-1}, approximately 46-fold slower than WT FTase. In summary, mutations in the PPi binding pocket have little affect on the ability of the enzyme to react with FMP, indicating that these residues likely interact mainly with the β-phosphate of FPP−Mg^{2+} in the reactive ternary complex or chemical transition state.

To determine whether the effect of R291A on FMP turnover was related to impaired binding of the substrate, K_D values for FMP were measured for WT, R291A, and R291Q FTase by equilibrium dialysis (Figure 7, Table 3). WT has a K_D value for FMP dissociation of 92 ± 15 nM, compared to 10 nM with FPP, again illustrating the importance of hydrophobic interactions with the farnesyl chain for high-affinity binding. The R291Q and R291A mutations enhance the affinity of FMP modestly, by 1.6−2.7-fold (Table 3). Therefore, the decreased ability of R291A FTase to catalyze the single turnover reaction with FMP cannot be related to a loss of FMP binding affinity. Comparison of R291A and R291Q FTase indicates that these mutants bind FMP with a similar affinity but do not catalyze farnesylation with similar efficiencies. This disparity may be related to differences in the conformation of bound FMP with the alanine replacement versus the glutamine side chain. It is interesting to note that the mutations at R291 decrease the FPP affinity (4−17-fold, Table 1) while increasing the FMP affinity. WT binds FPP 9-fold more tightly than FMP, while this discrimination is diminished in the R291A mutant and inversed with the R291Q mutant. These data further highlight the interaction of the R291β side chain with the β-phosphate of FPP in the WT enzyme.

Effect of Mutants on Product Release Kinetics. To fully characterize the kinetics of the R291β and K294β mutants relative to WT, multiple turnover kinetics at saturating substrate concentrations (k_{cat}) were measured. The rate-limiting step for WT under these conditions is dissociation of the farnesylated peptide product (*8*). Values for this rate constant are listed in Table 1. WT has a k_{cat} of 0.022 ± 0.001 s^{-1} (*8*). All mutations studied alter this value little relative to WT. Mutations at position 294 have no effect on the value of k_{cat}, while the k_{cat} for mutations at 291 varies from a low of 0.013 s^{-1} (2-fold decrease) for R291A to a high of 0.064 s^{-1} (3-fold increase) for R291Q. These slight variations do not correlate with changes in either the peptide or FPP affinity. These results indicate that the side chains of R291β and K294β do not play a direct role in controlling the dissociation rate constant of the farnesylated peptide product. These results are consistent with preliminary measurements indicating that the rate constant of PPi release for WT in the presence of Mg^{2+} is equal to or faster than k_{chem} (Pais, Bowers, Fierke, unpublished results). Upon release of PPi, the diphosphate binding pocket interacts with a FPP molecule that binds to the E−product complex and facilitates product dissociation (*23*, *28*).

DISCUSSION

The Chemical Transition State of FTase. The picture that is emerging from the collection of FTase crystal structures, metal substitution studies, mutational analyses, and kinetic examination of the chemical reaction (*8*, *11*, *19*, *22*−*24*, *29*, *30*) is one of a transition state that is intricately stabilized by a number of factors. The timing of the interactions of side chains and metals with substrates, which are critical for facilitating the conformational movements needed to bring the reactive elements close enough for catalysis, appears to be tightly orchestrated. The following hypothesis presents a chronological view of events that may occur leading up to the transition state: (1) The enzyme first binds FPP and sequesters the PPi moiety within the diphosphate binding pocket. This limits the interaction of the Mg^{2+} ion with the PPi moiety prior to binding of the peptide CaaX sequence. Within the enzyme active site, premature interaction with Mg^{2+} could result in catalysis of hydrolysis of FPP with the formation of PPi and farnesol (hydroxide derivative of the farnesyl chain), an unreactive molecule for the farnesylation reaction (unpublished results). The positively charged residues of the PPi binding pocket, as demonstrated by the K_{Mg} data (Figure 4), attenuate the affinity of FPP for Mg^{2+} when the substrate is bound to the WT enzyme. (2) The CaaX peptide substrate binds to the E−FPP complex with the Zn^{2+} coordinating the thiolate, creating the potent nucleophile in this reaction, as observed by X-ray crystallography, absorption spectroscopy of Co^{2+}−FTase, and extended X-ray absorption fine structure (EXAFS) studies (*8*, *11*, *14*, *30*). The Zn^{2+} binding geometry in the free enzyme is tetrahedral, interacting with His362β, C299β, one oxygen of D297β, and either a second oxygen of D297β or a water molecule (*30*, *31*). Upon binding the peptide, one ligand (either water or an oxygen from D297β) is displaced by the peptide cysteine thiolate, so the zinc polyhedron retains the tetrahedral geometry typically adopted by catalytic zinc ions. The side chain carboxylate of D297β is in close proximity to the carboxylate of D352β (within ~3.5 Å) (Figure 2B), a moiety that has been implicated in binding Mg^{2+} by mutational studies (*22*). (3) The change in interaction of D297β with Zn^{2+} may trigger the formation of the high-affinity Mg^{2+} site and rotation of the prenyl chain of FPP. After peptide binds, the prenyl chain of FPP rotates to the conformation observed in the crystal structure of the bound product (*23*). This positions the C-1 of FPP near the sulfur of the peptide substrate to facilitate nucleophilic attack. This conformational change also alters the position of the diphosphate moiety of

FPP, moving it sufficiently close to the side chain of D352β such that a higher affinity octahedral Mg^{2+} site (see Figure 2B) is proposed to form from two oxygens of the diphosphate of FPP, two oxygens from the side chain of D352β, one oxygen of the carboxylate side chain of the zinc ligand, D297β, and one water molecule held in place with hydrogen bonds to nearby lysine side chains. This type of bimetal catalytic site in which two metals are bridged by a common aspartate residue is not uncommon in nature. Examples of this type of metal site are found in enzymes such as adenylate cyclase (*18*), involved in the conversion of ATP to cyclic adenosine monophosphate, and enolase, an enzyme that catalyzes the dehydration of 2-phosphoglycerate (*15*). In these enzymes, one of the metal ions occupies a high-affinity site with a tetrahedral geometry (typically Mg^{2+}, Mn^{2+}, or Zn^{2+}), while the second metal ion occupies a low-affinity site with an octahedral geometry. In this type of active site, the low-affinity metal ion is proposed to bind only in the presence of substrate, that is, in a transient manner (*32*). This behavior is analogous to our hypotheses on metal binding in FTase. (4) In the final step, the active E−peptide−FPP−Mg^{2+} complex efficiently catalyzes thioether bond formation with a dissociative transition state with developing positive charge on C-1 and negative charge on the diphosphate leaving group (*8*).

Role of Positive Charge in the Diphosphate Binding Pocket. The positively charged residues of the diphosphate binding pocket play several key roles in the FTase-catalyzed farnesylation reaction, including the following. (1) Binding of FPP: According to the K_D values for FPP binding, the side chains of R291β and K294β provide 3−4 kJ/mol of binding energy. The size of this energy contribution to FPP binding is consistent with a solvent-exposed charge−charge interaction (*27*). The modest effect of the mutations on the FMP binding constants and farnesylation rate constant indicate that these residues mainly interact with the β-phosphate of FPP. (2) Attenuation of Mg^{2+} affinity: The R291A and R291Q mutants lower the $K_{1/2}$ for Mg^{2+} by 20−40-fold, indicating that this side chain in WT FTase decreases the apparent Mg^{2+} affinity of FPP up to 9.7 kJ/mol (R291Q, Table 2). As discussed, this attenuation is advantageous to the reaction by limiting the interaction of the PPi moiety with Mg^{2+} prior to peptide binding. It is interesting to note that free FPP has a K_{Mg} value at pH 7.8 of 0.12 mM (*22*), similar to the pH-independent $K_{1/2}$ values measured for the R291β mutants (Table 2). This correlation suggests that in the R291β mutants the diphosphate moiety is not anchored in the diphosphate binding pocket and has greater access to Mg^{2+}. (3) Stabilization of the charge on the diphosphate: A shift of the Mg^{2+}-dependent pK_a value to higher pH in the R291A and R291Q mutants is indicative of a role for this side chain in stabilizing the deprotonated form of FPP (see Scheme 1). In the absence of the positive charge of the arginine side chain, the deprotonated form of bound FPP is destabilized. Similarly, the positive charge of the R291 side chain is positioned to stabilize the developing negative charge on the diphosphate leaving group in the transition state. Deletion of this side chain removes this stabilization leading to the significant reduction in the catalytic rate constant for these mutant enzymes. The difference in the pK_a value for R291Q relative to R291A FTase indicates that the positive charge of the arginine side chain is not the only factor that contributes to diphosphate charge stabilization. The conformational movement of the diphosphate group toward the high-affinity Mg^{2+} site must also contribute to this stabilization. The bulkier glutamine side chain replacement at R291 may make a significant contribution to facilitating this conformational change through steric interactions.

Previously, the role of other diphosphate binding pocket residues, including K164α, H248β, and Y300β, in the FTase-catalyzed reaction was examined by mutagenesis (*24*). Except for Y300F FTase, mutations at these positions decrease k_{chem} either in the presence or in the absence of Mg^{2+} to a similar degree as the R291β and K294β mutants. The side chain of Y300β forms a hydrogen bond with the α-phosphate of FPP and is important for stabilizing the active conformation as well as developing charge in the transition state (*24*). However, these mutations exert a smaller affect on the FPP affinity, the $K_{1/2}$ for Mg^{2+}, and the Mg^{2+}-dependent pK_a for deprotonation of the diphosphate moiety. This comparison highlights the major role of R291β and K294β in attenuation of Mg^{2+} affinity and in stabilization of the developing negative charge on the diphosphate moiety in the chemical transition state. With the exception of Y300β, which is proposed to interact with the α-phosphate, the side chains in the diphosphate binding pocket predominantly interact with the β-phosphate of FPP in the active conformation.

FTase May Contain a "P-Loop"-like Motif. The data presented on mutants of R291β and K294β indicate that these residues act in concert with Mg^{2+} to facilitate catalysis by stabilization of the developing negative charge on the diphosphate leaving group or by positioning the bound FPP or both. Similar roles for conserved arginine and lysine side chains are predicted for enzymes such as shikimate kinase (*33*) and undecaprenyldiphosphate synthase (UPS) (*25*). In both enzymes, the substrate PPi moiety (for UPS, this relates to one of the PPi moieties in this two-substrate enzyme) is sandwiched between a catalytically important Mg^{2+} ion and conserved arginine or lysine residues or both in regions termed either a LID domain (shikimate kinase) or a structural P-loop (UPS). UPS catalyzes the sequential cis condensation of isopentyldiphosphate and farnesyldiphosphate to form undecaprenyldiphosphate. Therefore, the P-loop structure and reaction is more easily related to FTase since the substrates are similar. As with FTase, Mg^{2+} is important for catalysis by UPS, even though this *cis*-prenyl elongating enzyme also lacks the signature DDXXD Mg^{2+}-binding motif (*25*). The P-loop structure of UPS is located at the N-terminus of a helix and has the sequence DGNGR (*25*). It is thought to play an important role in substrate recognition and positioning of the PPi leaving group, facilitating the condensation of the two substrates. In FTase, R291β and K294β are similarly located in a loop structure with an amino acid sequence of **EG**GF**QGR**CNKL. Both of these loops can be represented by the sequence motif (D/E)G$X_{(0-2)}$(N/Q)GR. Although the FTase loop is not identical in sequence or size to that of UPS, the glycine residues in this loop region in FTase afford a certain level of structural flexibility that could be conducive to the movement of the diphosphate moiety away from this region to form the reactive ternary complex. It is conceivable that this loop may close around the active site during the chemical reaction to limit the solvent exposure of the reactive species. In addition, this hypothesized flexibility would also allow R291β to play a role in PPi

stabilization even when this moiety moves toward the Mg^{2+} binding site. The side chain of R291 could move along with PPi, maintaining hydrogen bonding and salt bridge interactions. This movement would maintain the positively charged environment that stabilizes the leaving group. In examination of the current proposed model for the active ternary complex including the Mg^{2+} binding site (Figure 2B), the side chains of R291β and K294β are located 7−9 Å away from the nearest oxygen atom of the β-phosphate. This initial model was prepared assuming that the protein structure was static. However, the current data suggest that the side chains of R291β and K294β should move toward the diphosphate moiety in the active ternary complex. The mobility of this "P-loop" may be important for accomplishing the new conformation.

In conclusion, FTase employs a combination of reaction characteristics found in diverse enzymes such as adenylate kinase (metal binding site) and UPS (P-loop) in a synergistic manner to efficiently catalyze sulfur alkylation, using an elegant balance of metal coordination and charge stabilization.

ACKNOWLEDGMENT

We thank Dr. Jennifer Pickett for helpful discussions and insight.

REFERENCES

1. Roskoski, R. (2003) Protein prenylation: a pivitol posttranslational process, *Biochem. Biophys. Res. Commun. 303*, 1−7.
2. Sinensky, M. (2000) Functional aspects of polyisoprenoid protein substituents: roles in protein−protein interaction and trafficking, *Biochim. Biophys. Acta 1529*, 203−209.
3. Resh, M. (1996) Regulation of Cellular Signaling by Fatty acid acylatation and prenylation of signal transduction proteins, *Cell. Signalling 8*, 403−412.
4. Seabra, M. (1998) Membrane association and targeting of prenylated Ras-like GTPases, *Cell. Signalling 10*, 167−172.
5. Adjei, A. (2001) Blocking Oncogenic Ras Signaling for Cancer Therapy, *J. Natl. Cancer Inst. 93*, 1062−1074.
6. Sinensky, M. (2000) Recent advances in the study of prenylated proteins, *Biochim. Biophys. Acta 1484*, 93−106.
7. Brunner, T., Hahn, S., Gupta, A., Muschel, R., McKenna, W., and Bernhard, E. (2003) Farnesyltransferase inhibitors: an overview of the results of preclinical and clinical investigations, *Cancer Res. 63*, 5656−5668.
8. Huang, C.-c., Hightower, K., and Fierke, C. (2000) Mechanistic studies of rat protein farnesyltransferase indicate an associative transition state, *Biochemistry 39*, 2593−2602.
9. Furfine, E., Leban, J., Landavazo, A., Moomaw, J., and Casey, P. (1995) Protein farnesyltransferase: kinetics of farnesyl pyrophosphate binding and product release, *Biochemistry 34*, 6857−6862.
10. Dolence, J., and Poulter, C. (1995) A mechanism for posttranslational modifications of proteins by yeast protein farnesyltransferase, *Proc. Natl. Acad. Sci. U.S.A. 92*, 5008−5011.
11. Hightower, K., Huang, C.-c., Casey, P., and Fierke, C. (1998) H-Ras peptide and protein substrates bind protein farnesyltransferase as an ionized thiolate, *Biochemistry 37*, 15555−15562.
12. Rozema, D., and Poulter, C. (1999) Yeast protein farnesyltransferase. pK_as of peptide substrates bound as zinc thiolates, *Biochemistry 38*, 13138−13146.
13. Park, H., Boduluri, S., Moomaw, J., Casey, P., and Beese, L. (1997) Crystal structure of protein farnesyltransferase at 2.25 angstrom resolution, *Science 275*, 1800−1804.
14. Long, S., Casey, P., and Beese, L. (2000) The basis for K−Ras4B binding specificity to protein farnesyltransferase revealed by 2 Å resolution ternary complex structures, *Struct. Fold. Des. 8*, 209−222.
15. Poyner, R., Cleland, W., and Reed, G. (2001) Role of metal ions in catalysis by enolase: an ordered kinetic mechanism for a single substrate enzyme, *Biochemistry 40*, 8009−8017.
16. Kemp, L., Bond, C., and Hunter, W. (2002) Structure of 2C-methyl-D-erythritol 2,4-cyclodiphosphate synthase: an essential enzyme for isoprenoid biosynthesis and target for antimicrobial drug development, *Proc. Natl. Acad. Sci. U.S.A. 99*, 6591−6596.
17. Tarshis, L., Yan, M., Poulter, C., and Sacchettini, J. (1994) Crystal structure of recombinant farnesyl diphosphate synthase at 2.6-Å resolution, *Biochemistry 33*, 10871−10877.
18. Tesmer, J., Sunahara, R., Johnson, R., Gosselin, G., Gilman, A., and Sprang, S. (1999) Two-metal-Ion catalysis in adenylyl cyclase, *Science 285*, 756−760.
19. Saderholm, M., Hightower, K., and Fierke, C. (2000) Role of metals in the reaction catalyzed by protein farnesyltransferase, *Biochemistry 39*, 12398−12405.
20. Long, S., Hancock, P., Kral, A., Hellinga, H., and Beese, L. (2001) The crystal structure of human protein farnesyltransferase reveals the basis for inhibition by CaaX tetrapeptides and their mimetics, *Proc. Natl. Acad. Sci. U.S.A. 98*, 12948−12953.
21. Kral, A., Diehl, R., deSolms, S., Williams, T., Kohl, N., and Omer, C. (1997) Mutational analysis of conserved residues of the beta-subunit of human farnesyl: protein transferase, *J. Biol. Chem. 272*, 27319−27323.
22. Pickett, J., Bowers, K., and Fierke, C. (2003) Mutagenesis Studies of Protein Farnesyltransferase Implicate Aspartate β352 as a Magnesium Ligand, *J. Biol. Chem. 278*, 51243−51250.
23. Long, S., Casey, P., and Beese, L. (2002) Reaction path of protein farnesyltransferase at atomic resolution, *Nature 419*, 645−650.
24. Pickett, J., Bowers, K., Hartman, H., Fu, H., Embry, A., Casey, P., and Fierke, C. (2003) Kinetic studies of protein farnesyltransferase mutants establish active substrate conformation, *Biochemistry 42*, 9741−9748.
25. Fujihashi, M., Zhang, Y., Higuchi, Y., Li, X., Koyama, T., and Miki, K. (2001) Crystal structure of cis-prenyl chain elongating enzyme, undecaprenyl diphosphate synthase, *Proc. Natl. Acad. Sci. U.S.A. 98*, 4337−4342.
26. Zimmerman, K., Scholten, J., Huang, C., Fierke, C., and Hupe, D. (1998) High-level expression of rat farnesyl: protein transferase in *Escherichia coli* as a translationally coupled heterodimer, *Protein Expression Purif. 14*, 395−402.
27. Fersht, A., Shi, J.-P., Knills-jones, J., Lowe, D., Wilkinson, A., Blow, D., Brick, P., Carter, P., Waye, M., and Winter, G. (1985) Hydrogen bonding and biological specificity analysed by protein engineering, *Nature 314*, 235−238.
28. Tschantz, W., Furfine, E., and Casey, P. (1997) Substrate binding is required for release of product from mammalian protein farnesyltransferase, *J. Biol. Chem. 272*, 9989−9993.
29. Huang, C.-c., Casey, P., and Fierke, C. (1997) Evidence for a catalytic role of zinc in protein farnesyltransferase, *J. Biol. Chem. 272*, 20−23.
30. Tobin, D., Pickett, J., Hartman, H., Fierke, C., and Penner-Hahn, J. (2003) Structural Characterization of the zinc site in protein farnesyltransferase, *J. Am. Chem. Soc. 125*, 9962−9969.
31. Hightower, K., and Fierke, C. (1999) Zinc-catalyzed sulfur alkylation: insights from protein farnesyltransferase, *Curr. Opin. Chem. Biol. 3*, 176−181.
32. Cowan, J. (2002) Structural and catalytic chemistry of magnesium-dependent enzymes, *BioMetals 15*, 225−235.
33. Gu, Y., Reshetnikova, L., Li, Y., Wu, Y., Yan, H., Singh, S., and Ji, X. (2002) Crystal structure of shikimate kinase from Mycobacterium tuberculosis reveals the dynamic role of the LID domain in catalysis, *J. Mol. Biol. 319*, 779−789.

BI049822P